

http://pubs.acs.org/journal/aesccq Article

# Metal Oxide Particles as Atmospheric Nuclei: Exploring the Role of Metal Speciation in Heterogeneous Efflorescence and Ice Nucleation

Zachary R. Schiffman, Marium S. Fernanders, Ryan D. Davis, and Margaret A. Tolbert\*



Cite This: ACS Earth Space Chem. 2023, 7, 812–822



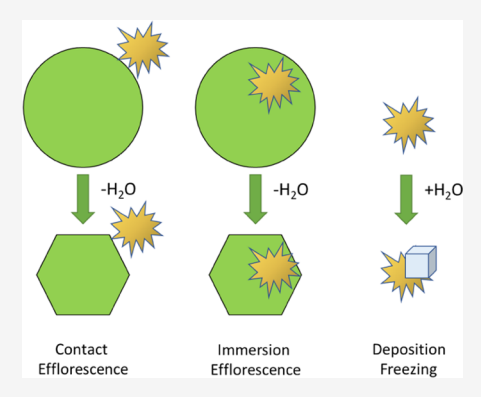
**ACCESS** I

III Metrics & More

Article Recommendations

Supporting Information

ABSTRACT: Mineral dust can indirectly impact climate by nucleation of atmospheric solids, for example, by heterogeneously nucleating ice in mixed-phase clouds or by impacting the phase of aerosols and clouds through contact nucleation. The effectiveness toward nucleation of individual components of mineral dust requires further study. Here, the nucleation behavior of metal oxide nanoparticle components of atmospheric mineral dust is investigated. A long-working-distance optical trap is used to study contact and immersion nucleation of ammonium sulfate by transition-metal oxides, and an environmental chamber is used to probe depositional ice nucleation on metal oxide particles. Previous theory dictates that ice nucleation and heterogeneous nucleation of atmospheric salts can be impacted by several factors including morphology, lattice match, and surface area. Here, we observe a correlation between the cationic oxidation states of the metal oxide heterogeneous nuclei and their effectiveness in causing nucleation in both contact efflorescence mode and



depositional freezing mode. In contrast to the activity of contact efflorescence, the same metal oxide particles did not cause a significant increase in efflorescence relative humidity when immersed in the droplet. These experiments suggest that metal speciation, possibly as a result of cationic charge sites, may play a role in the effectiveness of nucleation that is initiated at particle surfaces.

KEYWORDS: contact efflorescence, immersion efflorescence, depositional ice nucleation, metal oxides, surface potential, ammonium sulfate, aerosol interfaces

# 1. INTRODUCTION

Mineral dust is a significant aerosol component of the atmosphere with an estimated source of approximately 2000 teragrams emitted per year. Arid regions including deserts account for a large source of mineral dust, and particles can travel distances of thousands of kilometers over the course of several days. It is estimated that approximately one-quarter of mineral dust emissions originate from anthropogenic and agricultural activity, while three-quarters originate from natural sources. However, due to a combination of agricultural expansion and increased likelihood of drought due to climate change, sources of atmospheric dust loading have been shown by aerosol optical depth observations to have increased by approximately 5% per year since 2000. As such, it is vital to follow and identify the impacts of mineral dust on atmospheric processes.

It is well established that atmospheric aerosol particles including mineral dust play a significant role in atmospheric radiative balance.<sup>4</sup> In addition to direct effects, mineral dust can indirectly impact climate by nucleation of atmospheric solids. For example, field studies of cirrus cloud residuals by Cziczo et al. reveal that over 60% of heterogeneous ice residuals from cloud encounters consist of metals and minerals.<sup>5</sup> Mineral dust particles may also impact the phase

of aerosols and clouds through collisions resulting in contact efflorescence, where efflorescence is defined as the crystallization of dissolved solute.  $^{6-11}$ 

Past laboratory studies have shown that mineral dust can be an effective and common ice nucleus. <sup>12,13</sup> Some models suggest that freezing of mineral dust in the immersion mode is the primary route of atmospheric ice nucleation, and several freezing studies have been performed on mineral dusts, including illite, montmorillonite, Arizona Test Dust, and kaolinite in the immersion mode as well as in the deposition mode. <sup>14–18</sup> In particular, it has been shown that feldspars, notably alkali (sodium- and potassium-containing) feldspars, are outstanding ice nuclei and may be responsible for the excellent ice nucleation properties of mineral aerosols, both as deposition nuclei and in the immersion mode. <sup>19–22</sup> Many factors have been shown to contribute to and impact ice nucleation, such as surface defects, cracks, and pores. <sup>23–26</sup>

Received: December 2, 2022 Revised: March 16, 2023 Accepted: March 17, 2023 Published: March 30, 2023





Other potential factors include particle morphology, composition, and the presence of organic coatings. The focus of the present work is a systematic study regarding a previously unreported trend as a function of the metal oxide oxidation state. Future studies could attempt to link oxidation state and other known ice-nucleating parameters to gain more molecular insight.

In addition to ice nucleation, studies have shown that mineral dust and its components can induce heterogeneous efflorescence of common atmospheric salts. Ushijima et al. displayed evidence that common mineral dusts such as illite and montmorillonite can instigate heterogeneous efflorescence of ammonium sulfate (AS) and sodium chloride droplets *via* both immersion and contact modes at higher relative humidity than that of homogeneous efflorescence; that study found only a small impact from immersion efflorescence and a much larger influence from contact nucleation.

While the previous studies make it clear that mineral dust can provide excellent nucleation sites for heterogeneous nucleation in both the freezing and efflorescence modes, the role of the various components of mineral dust is still uncertain, as is the nucleation mechanism. Han and Martin have shown that inclusions of Al<sub>2</sub>O<sub>3</sub>, TiO<sub>2</sub>, and ZrO<sub>2</sub> can act as heterogeneous nuclei (HN) for efflorescence when internally mixed with droplets of ammonium sulfate. In the studies by Han and Martin, their inclusion raised the relative humidity of efflorescence (ERH) by up to 30% relative to homogeneous efflorescence, *via* immersion of the metal oxide nanoparticles within the salt droplet.<sup>27</sup> However, contact nucleation in particular lacks experimental study for metal oxide particles. This is true in the context of contact ice nucleation as well as for the contact efflorescence of salts.

To address these knowledge gaps, this study examined heterogeneous nucleation caused by metal oxide components of mineral dust. Here, the umbrella term heterogeneous nuclei refers to particles that can act as contact efflorescence nuclei, immersion efflorescence nuclei, or deposition ice nuclei. Depositional ice nucleation is studied on five mineral oxide particles, and the ice saturation ratio,  $S_{ice}$ , required for nucleation is reported. For these studies, an optical microscope is utilized, equipped with an environmental chamber to probe depositional ice nucleation on single particles deposited on a plate. Further, the same five mineral oxide particles are used to probe contact and immersion efflorescence of ammonium sulfate. A long-working-distance single-particle optical levitator is used to trap aqueous droplets in a flow cell and induce contact nucleation with the metal oxide nanoparticles. The optical levitator is used to study single droplets suspended in air, allowing observations of single collisions with single droplets. Immersion efflorescence is also studied with single droplets by allowing several collisions to occur before lowering the relative humidity (RH). Finally, the effectiveness of mineral oxides toward ice nucleation and contact efflorescence are compared to explore the driving forces of nucleation. Although our samples are not directly representative of atmospheric mineral dust, which possesses many metals with varying oxidation states, the purpose of this study is to identify the nucleation results of the metal oxide components of mineral dust samples that could be found in the atmosphere and to identify trends of nucleation activity.

#### 2. EXPERIMENTAL SECTION

**2.1. Metal Oxides and Materials.** Common metals are known to easily oxidize in atmospheric conditions; as such, this study investigated stable oxides of common metals. Nontoxic metal oxide nanoparticles of transition metals were utilized as heterogeneous nuclei (HN). The species were chosen for their discovery as effective ice nuclei or abundance in atmospheric aerosol and selected so that the suite of nuclei possessed a range of metal cation oxidation states in the ionic oxides. Their ability to support depositional ice nucleation as well as contact efflorescence of ammonium sulfate salt was probed. Metallic nanoparticles linked to well-known toxicity effects were not included in the studies.

The ammonium sulfate (99.8% purity) used in this study was acquired from Fisher Chemical. The zinc oxide, copper (II) oxide, and iron (III) oxide were acquired from Sigma-Aldrich with stated diameters of <100, <50, and <50, nm, respectively. The titanium (IV) oxide powder, also acquired from Sigma-Aldrich, had an unspecified particle size, with an average particle diameter less than 5000 nm according to manufacturer specification. Vanadium (V) oxide was purchased from Nanoshel at 99.9% purity at diameters of <100 nm. All aqueous or water slurry solutions were prepared using high-performance liquid chromatography (HPLC)-grade water from Fisher Chemical. Compressed nitrogen gas canisters used as carrier gas and for relative humidity (RH) control were purchased from Airgas.

A scanning mobility particle sizer (SMPS) was used to attain the size distribution profiles for the five species of metal oxide heterogeneous nuclei. The SMPS instrument consists of a differential mobility analyzer (DMA) (TSA Electrostatic Classifier Model 3080 and TSI Long DMA Model 3081) utilizing a Polonium-210 neutralizer, connected with 10" rubber tubing to a condensation particle counter (CPC) (TSI Model 3775). For each of the five metal oxides, a 0.5% colloidal slurry by weight was prepared in water and aerosolized using a medical-grade nebulizer. The aerosols then entered a silica-gel diffusion drier before entering the SMPS. A LabView program processed the data, allowing for analysis of size distributions. It should be noted that we do not have shape information on the aerosolized dried particles so the assumption of spherical particles may lead to significant errors in size. The size distribution profiles can be seen in Figure S1. The profiles varied in size, with mode diameters ranging between 55 and 310 nm. Three of the profiles were unimodal, while the zinc and titanium oxides were multimodal. The mode diameters recorded with the SMPS are ~5 times larger than the expected manufacturer dry size. The increase in size could be due to the hydration and subsequent drying of the particles, their nonsphericity, or particle agglomeration.

In contrast to the aerosolized particles, the agglomerates produced in the cold cell have diameters of >100  $\mu$ m. Although the physical shape and size of the metal oxide material are different in the two experimental modes (ice nucleation  $\nu$ s heterogeneous efflorescence), the goal of this paper is to identify overall trends regarding the potential role of oxidation state, and less so to directly compare the two modes of nucleation. The five metal oxide slurries were imaged using the cold-cell optical microscope, described in Section 2.2.1; the images are seen in Figure S2. In addition to microscope imaging, the five oxides were also spectrally observed using a second imaging instrument, an Oriba LabRAM HR Evolution

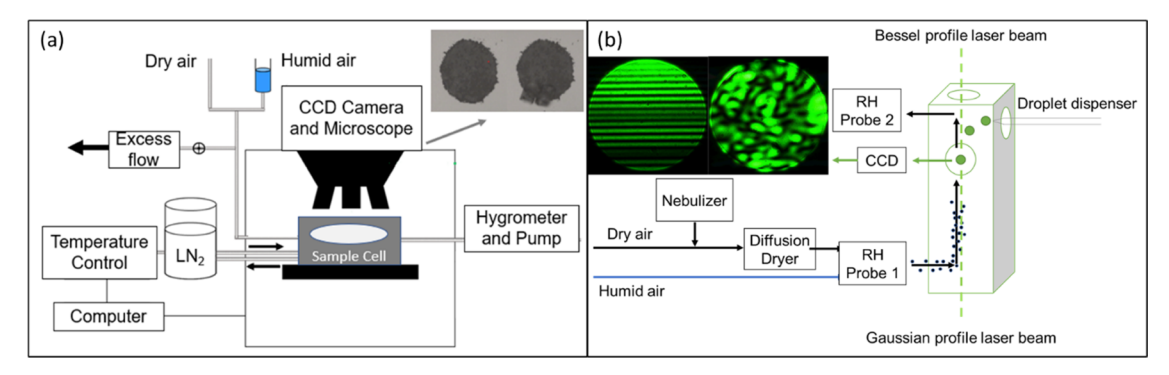


**Figure 1.** ((a) Left) Simplified schematic of the cold-cell microscopy chamber, adapted from Fernanders et al.<sup>31</sup> The temperature is controlled by an input of liquid nitrogen, and the RH is controlled by a combination of dry and wet gas flow. The sample is monitored by an optical microscope and a CCD camera. ((b) Right) Simplified schematic of optical levitator cell, adapted from Ushijima et al.<sup>10</sup> Included with the CCD camera is the far-field imaging of levitated ammonium sulfate before (left) and after (right) contact efflorescence with a zinc oxide HN.

Raman Spectrometer belonging to the Raman Microspectroscopy Lab at the University of Colorado Boulder. For both instruments, the slurries were dried on their slides before imaging. The imaging as well as the spectra allowed for confirmation of the samples' purity as well as their crystallinity. The  ${\rm TiO}_2$ ,  ${\rm ZnO}$ , and  ${\rm CuO}$  samples were confirmed, respectively, to be crystalline samples of anatase, synthetic zincite, and synthetic tenorite by the RRUFF database, matching the published Raman spectra. The  ${\rm V_2O_5}$  and  ${\rm Fe_2O_3}$  (maghemite) samples were confirmed as crystalline forms from other literature spectra. The Raman spectra are also displayed in Figure S2.

**2.2. Experimental Chambers.** Schematic diagrams of the experimental chambers used in the present study are shown in Figure 1. Ice nucleation experiments were performed in an optical microscope chamber shown in Figure 1a, while efflorescence studies were performed in an optical levitation cell, Figure 1b. Both experiments are detailed briefly below. The two instruments allow for observation of distinct forms of nucleation, and as such provide information together which could not be retrieved from one alone. In previous work, we have used the two instruments in tandem to investigate efflorescence patterns of Mars-relevant chlorate salts.<sup>31</sup> In that study, we found that the two instruments gave consistent results, for example that aqueous sodium chlorate droplets demonstrate homogeneous efflorescence at 25% RH at -6 °C in the cold cell and at 17  $\pm$  5% RH at 23 °C in the levitator. We also found consistent measurements from both instruments indicating that aqueous magnesium chlorate droplets do not demonstrate homogeneous efflorescence at any meaningful RH down to 3% RH.

2.2.1. Depositional Ice Nucleation Studied via Cold-Cell Microscopy. Ice nucleation experiments were performed using an environmental chamber, cooled by liquid nitrogen, and fitted with an optical microscope. The cold cell has been described in detail by Baustian et al.<sup>32</sup> Colloidal slurries of the five insoluble metal oxides were prepared, with concentrations ranging from 0.1 to 0.5% by weight depending on the opacity of the resulting solution. The colloids were shaken by hand and nebulized using pressurized nitrogen onto a quartz slide, and the slide was placed onto an iridium-coated steel block inside the chamber. The chamber was then sealed, and dry nitrogen passed over the droplets to evaporate the water prior to an experiment, leaving particle agglomerates on the slide.

The temperature inside the cell at the time of ice formation, and the frost point read from the hygrometer (Buck Research

Instruments Chilled Mirror Hygrometer CR-1A), are used to calculate the onset ice saturation ratio ( $S_{\rm ice}$ ) values for each of the metal oxides, where  $S_{\rm ice}$  is calculated as the ratio between the amount of water vapor in the air ( $P_{\rm H_2O}$ ) to the equilibrium vapor pressure of ice at that same temperature T (VP<sub>ice</sub>)

$$S_{\text{ice}}(T) = \frac{P_{\text{H}_2\text{O}}(T)}{VP_{\text{ice}}(T)}$$

The microscope is focused onto dried crystals of the metal oxide atop the slide, allowing visual studies as temperature and RH within the cell were changed. The humidity in the cell is controlled by passing the carrier gas flow through a glass bubbler flask filled with water, after which it was combined with a dry flow. The flows were held constant during an experiment to produce a constant partial pressure of water in the system. The temperature controller uses liquid nitrogen to cool the block inside the cell. As the temperature in the cell is lowered, the RH increases. In a typical experiment, temperature was lowered at a rate of -10 °C/min until  $S_{ice}$ approached 1.0. Then, the rate of cooling rate was lowered to  $-0.5~^{\circ}\text{C/min}$  and lowered once more to  $-0.2~^{\circ}\text{C/min}$  when Sice approached 1.2, until ice crystals were spotted growing on the metal oxide agglomerates. At that point, the temperature of the cell was raised at a rate of 10 °C/min until the ice crystals sublimed. In every case in which ice was observed, sublimation of the ice revealed that nucleation had occurred on the metal oxide and not the quartz substrate.

2.2.2. Heterogeneous Efflorescence of Levitated Ammonium Sulfate Droplets. Contact efflorescence was studied using an optical levitator as described in detail by Davis et al. In brief, a beam from a neodymium-doped yttrium aluminum garnet (Nd:YAG) green laser is split into two counterpropagating beams. The upward beam possesses a Gaussian profile, while the downward beam possesses a Bessel profile. The radiation pressure from the laser, in addition to a controlled upward flow of gaseous nitrogen, balances against the force of gravity to vertically stabilize an aqueous droplet inside of the levitator flow cell. Increased axial stability is provided by the Bessel beam.

The RH in the cell is controlled by passing a fraction of the nitrogen gas flow through a glass bubbler flask filled with water. Mass flow controllers are used to vary the ratio of dry air to wet air, allowing manual control of the relative humidity in the flow cell. The humidity is then measured by RH probes (Vaisala HMP60 or Vaisala HMP110) at both the entrance and exit to

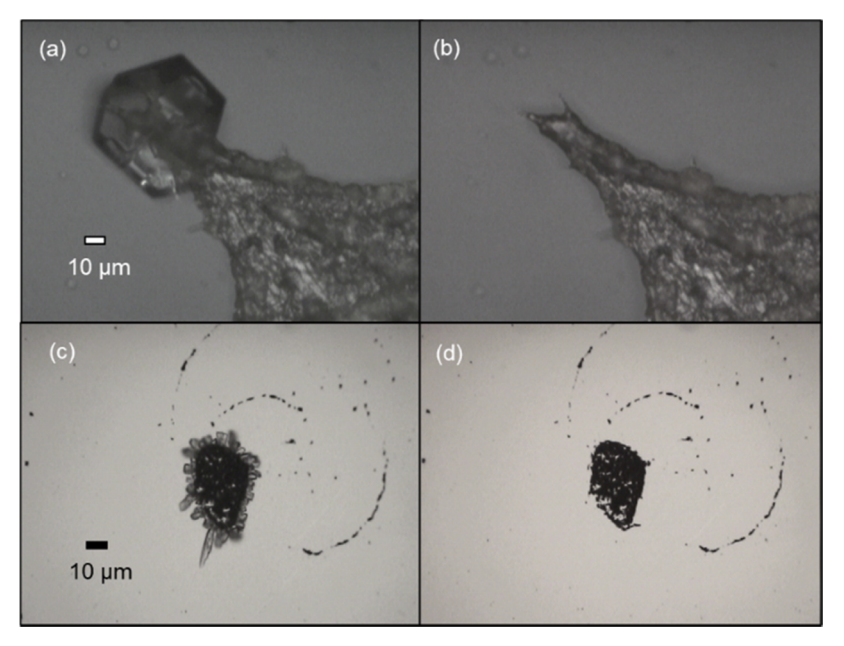


Figure 2. (a) Ice formation around an agglomerate of vanadium (V) oxide at -35.49 °C and  $S_{\rm ice} = 1.054$ ; (b) ice sublimation from the dry metal oxide agglomerate at room temperature, approximately 25 °C; and (c) ice formation on copper (II) oxide at -36.39 °C and  $S_{\rm ice} = 1.265$ , and (d) after warming to 25 °C.

the flow cell. The RH inside the cell is reported as the average value measured by the two RH probes. Discussion of error can be found in the Supporting Information. This work was performed at ambient room temperature, approximately 27 °C.

To prepare aqueous salt droplets to be levitated, a 5% by weight salt solution of ammonium sulfate (AS) was filtered through a 45  $\mu$ m cellulose acetate filter and loaded into a MicroFab droplet dispenser (MJ-ABP-01-20). The dispenser generates droplets of the aqueous solution into the upward air flow inside the flow cell. The cell is then shifted on a horizontally sliding scale to center the falling salt droplets in the path of the laser, allowing a droplet to be trapped behind the cell window. The trapped AS droplets possess diameters of approximately 15  $\mu$ m.

To prepare the heterogeneous nuclei (HN), a 5% by weight metal oxide slurry was made with HPLC-grade water. The mixture is sonicated to disperse the insoluble particles. The slurry is loaded into a medical-grade nebulizer (Omron NE-U22), and aerosolized directly into the dry nitrogen air flow, where it is carried into a diffusion drier with RH < 10% to remove water and then into the flow cell to make contact with the levitated salt droplet.  $^6$ 

The stream of metal oxide particles in the upward gas flow are visible in the levitation cell window due to laser scattering. As revealed by studies using the same instrument and flow rate by Ushijima et al., for a trapped droplet introduced to a stream of HN for 60 s, the droplet is exposed to an average of approximately one collision every 10 s. The method of determining the heterogeneous relative humidity of contact efflorescence (CERH) was also adapted from Ushijima et al. Experiments were performed by levitating an ammonium sulfate droplet and setting the relative humidity (RH) greater than the homogeneous efflorescence RH of ammonium sulfate (36  $\pm$  2%) but lower than the deliquescence RH (80%).  $^{6,7}$  Metal oxide particles were then allowed to collide with the AS droplet.

In contact experiments, if contact efflorescence did not take place within 60 s (after approximately six collisions), the droplet was discarded by rapidly moving the stage, disrupting the radiative balance of the beams. For replicate observations, a new droplet was captured. Five trials were performed for each metal oxide pairing with ammonium sulfate at each relative humidity. The RH was then lowered and additional contact experiments were performed until an RH was reached where contact efflorescence was effective.

In immersion experiments, the ammonium sulfate droplet was allowed to remain in the particle stream for 30 s, at an RH approximately 10% greater than the observed CERH, as not to accidentally induce contact efflorescence. This resulted in approximately three collisions. The particle stream was then stopped, and the RH decreased at a rate of approximately 1% RH/min to probe efflorescence.

To confirm that a crystallization event has occurred, a CCD camera is utilized to observe the far-field imaging of the droplet. The Mie scattering of a spherical, aqueous droplet results in regularly spaced bands of light. After crystallization, the bands disappear and are replaced by random scattering patterns due to the crystal's asymmetric geometry. In addition, upon loss of water, the particle moves up vertically in the trap. Previous work with this instrument has used Raman spectrometry to confirm that the stochastic scattering image does correspond to a loss of water and does represent an efflorescence event.<sup>31</sup>

# 3. RESULTS AND DISCUSSION

**3.1. Depositional Ice Nucleation Studied** *via* **Cold-Cell Microscopy.** It is pertinent to note that the term "depositional nucleation" is used here to signify the formation of ice on the metal oxide agglomerate originating from the vapor form. However, recent studies suggest that, below water saturation, instead of water vapor depositing directly as ice onto the surface of the ice nuclei, there are condensation events in pores and surface imperfections that are followed by freezing

events. <sup>23,24</sup> For the purposes of this paper, the term deposition will still be used for simplification of language.

Typical ice nucleation experiments on vanadium (V) oxide and copper (II) oxide are shown in Figure 2. In this experiment, ice nucleated at  $S_{ice} = 1.054$  and 1.265 for vanadium and copper oxides, respectively. In Figure 2a,c, ice particles are visible in the center. In Figure 2b,d, after sublimation, the metal oxide nucleation sites remain. In all cases, ice particles were observed to nucleate on the metal oxide agglomerate and not on the quartz slide substrate, confirmed by the observed presence of a metal oxide agglomerate underneath each ice crystal after sublimation. Because ice nucleation is a stochastic process, it was not possible to know in advance which specific agglomerate would nucleate ice first in a set of nominally identical conditions. Therefore, images of the metal oxides are only available after ice nucleation. The goal of this paper is to address overall trends regarding large numbers of particle agglomerates under identical conditions, comparing different metal oxide species to each other rather than individual metal oxide agglomerates.

The results from the cold-cell experiments for the five metal oxides are summarized in Table 1. Each of the five metal oxides

Table 1. Depositional Ice Nucleation on Supermicron Deposited Particle Agglomerates

material	S <sub>ice</sub> value <sup>a</sup>	approximate diameter $(\mu m)^b$	refs for previous ice nucleation studies
$Fe_2O_3$	$1.14 \pm 0.027$	70	12, 37, 38
$V_2O_5$	$1.07 \pm 0.015$	100	
ZnO	$1.23 \pm 0.048$	130	
CuO	$1.24 \pm 0.045$	120	
$TiO_2$	$1.08 \pm 0.016$	50	

"Results from this study. Ice nucleation was observed between -35 and -40 °C for all metal oxides. The error signifies the standard deviation between the three trials for each metal oxide. <sup>b</sup>The reported diameters are the sizes of the particle agglomerates seen in Figure S2.

was shown to be a suitable heterogeneous nucleus for depositional ice nucleation, with average Sice values ranging from 1.07 to 1.24, all lower than the homogeneous value of approximately  $S_{\text{ice}} = 1.5.33$  These metal oxide compounds are also reasonably effective at depositionally forming ice when compared to other mineral ice nuclei at this temperature; Knopf and Koop found that Arizona Test Dust depositionally forms ice at  $S_{ice}$  between 1.05 and 1.45 at -33 °C, and Salam et al. found that kaolinite and montmorillonite form ice at  $S_{ice}$ 1.25 and 1.15, respectively, at −35 °C. <sup>34,35</sup> Further, secondary organic aerosols derived from  $\alpha$ -pinene have been shown to nucleate ice depositionally at higher Sice values, in the range from 1.35 to 1.45, displaying the effectiveness of these metal oxides.<sup>36</sup> The metal oxides observed in this study possess reasonably low  $S_{\rm ice}$  in the temperature range of -35 to  $-40~^{\circ}$ C, and therefore may be relevant to ice nucleation in an atmospheric context.

It has been previously shown that there is a correlation between ice nucleation ability and the crystal lattice match between the heterogeneous nucleus with structure of ice.<sup>39</sup> The calculation method employed is adapted from Davis et al. and is described in the Supporting Information.<sup>6,7</sup> Figure S3 is a plot of the ice saturation ratio  $\nu$ s the lattice mismatch between ice and the metal oxide crystals for the five metal oxides. In contrast to previous work, there does not appear to

be a correlation between lattice match and the ice saturation ratio among the five metal oxides. This is not entirely unexpected, as lattice match is not the only factor that determines the effectiveness of ice nucleation; Fitzner et al. summarize these other factors including local surface liquid ordering, density reduction of liquid, and the adsorption energy landscape. <sup>40</sup>

It has also previously been suggested that there could be a correlation between ice nucleation and the surface charge distribution on heterogeneous nuclei. Glatz and Sarupria used molecular dynamics simulations with silver iodide and water to posit that the orientation of the ionic charges affects the efficiency of ice nucleation; they found that ice nucleation occurred when the positive cation was positioned closer to the surface near the interface with water, and was inhibited when the negative anion was positioned higher. Studies by Zielke et al. further demonstrate the charge dependence of liquid water density profiles and the effect that it has on ice nucleation. <sup>42</sup>

Noting the effect that charge may have on ice nucleation, our  $S_{ice}$  values are plotted against the oxidation state of the metal oxide cations in Figure 3. A nonlinear negative

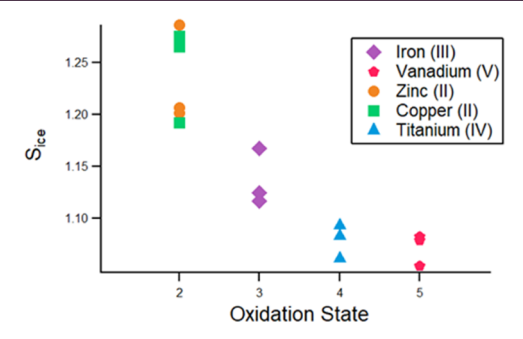


**Figure 3.** Ice saturation as a function of the oxidation state of the metal oxide cation. Each point represents a trial of one metal oxide agglomerate in the cold-cell chamber.

correlation is observed as the cation oxidation state of the metal oxide is increased. The crystals with highly oxidized metals show low Sice values and therefore high ice nucleation ability, and metals with low oxidation states show higher  $S_{ice}$ values and therefore lower ice nucleation ability. While this study did not take measurements of the surface potential of solid particles into account, this correlation may provide evidence for further charge dependence. In particular, the oxidation state of a metal may influence water adsorption at coordinatively unsaturated metal cation sites. 43 Ultimately, all five of the metal oxides act as efficient nuclei. The similarity in ice nucleation ability of copper (II) and zinc (II) oxides adds weight to the theorized relationship, and future studies would benefit from the investigation of other metal oxide particles with different oxidation states to determine if the trend continues and is robust.

Previous work performed by Kumar et al. investigated the effect of aqueous salt solutions on the immersion freezing of suspended mineral dust, finding that dilute acidic solutions (e.g., NH<sub>4</sub><sup>+</sup>) enhanced the ice nucleation ability of samples such as feldspars and kaolinite, implying an effect of hydrogen bonding on favorable ice nucleation. They concluded that solute-surface ion exchange in slightly acidic environments must be relevant to ice nucleation activity. Further work from Worthy et al. shows that ammonium sulfate boosts the ice nucleation activity of mineral dust while having no significant

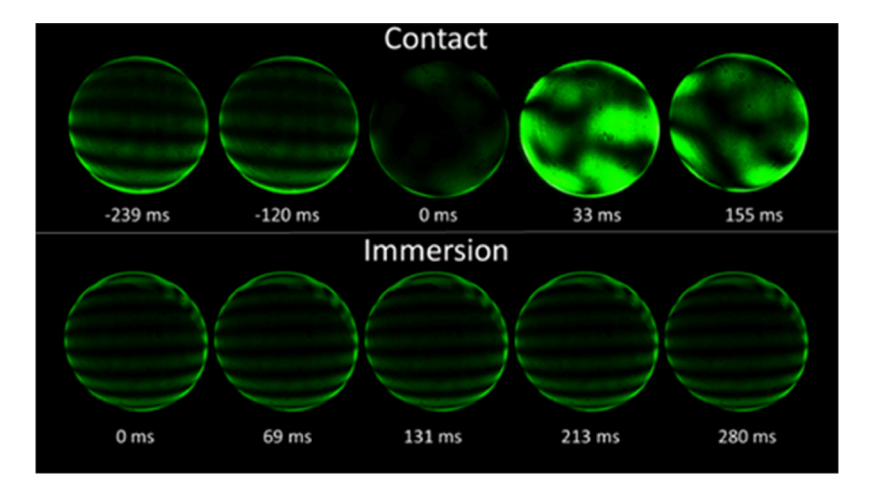


**Figure 4.** (Top) Droplet of AS before and after collision with an iron (III) oxide nanoparticle, at 54% relative humidity. (Bottom) Optically levitated droplet of ammonium sulfate internally mixed *via* immersion with iron (III) oxide nanoparticles, at 54% relative humidity. At the same RH, collision led to heterogeneous efflorescence while an internally mixed particle led to no change.

effect on most nonmineral nuclei, implying that the ubiquity of ammonium sulfate in atmospheric aerosol could increase the relevance of mineral dust in atmospheric ice nucleation.<sup>47</sup> It would be of interest to continue these studies of immersion freezing in aqueous salt solutions with the metal oxide components used in this study.

3.2. Heterogeneous Efflorescence of Levitated Ammonium Sulfate Droplets. The same five metal oxides were probed for their effectiveness in nucleating ammonium sulfate efflorescence. Figure 4 shows an example of how efflorescence is detected. The aqueous droplet displays a linear Mie pattern before efflorescing, after which point the ammonium sulfate crystal displays more chaotic imaging. In the top images of Figure 4, a droplet of AS is observed by the CCD camera at 54% RH, before and after collision with a  $Fe_2O_3$  nanoparticle (at t = 0 ms). In this experiment, contact efflorescence occurred at 54% RH. In the bottom images, a levitated droplet of AS has been internally mixed via immersion with approximately 3 particles of Fe<sub>2</sub>O<sub>3</sub> at approximately 65% RH, and then the RH lowered to 54%. At 54%, the same RH at which contact efflorescence occurred, no phase change was detected. Our indicator of crystallization is the same for all metal oxides. However, the results of the experiments (i.e., the ERH) are different for each metal oxide.

Figure 5 shows the fraction of collisions that resulted in contact efflorescence as a function of RH for each of the five metal oxides. A fraction of 0 signifies that no efflorescence events were observed under these conditions, while a fraction of 1 signifies that every observed contact trial between ammonium sulfate and the metal oxide led to efflorescence of the salt droplet. At high RH above 73%, none of the metal oxides induced contact efflorescence while at RH below 40%, each metal oxide induced contact efflorescence above the homogeneous ERH (~36%). For each metal oxide, a sigmoidal curve was fit to the data point using IgorPro (see Figure 5). The contact efflorescence relative humidity (CERH) is determined at the point where the sigmoid curve obtains an efflorescence probability fraction of 0.5. A high CERH value signifies that contact efflorescence of AS can occur in wetter air environments compared to homogeneous efflorescence. Note that the CERH values cannot exceed the deliquescence relative humidity of ammonium sulfate (80%), above which the crystalline phase is not sustainable.

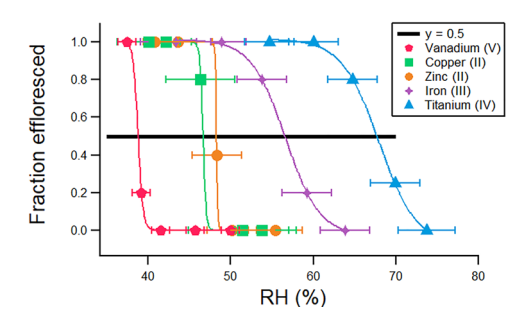


**Figure 5.** Five sigmoidal curve fits representing the fraction of collision events of AS with each respective metal oxide, which resulted in contact efflorescence, vs the relative humidity of contact efflorescence. The CERH is defined as the point where the sigmoidal fit crosses y = 0.5. Discussion of the error bars can be found in the Supporting Information.

Table 2 displays the calculated CERH of ammonium sulfate with each transition-metal oxide. It is seen that titanium (IV)

Table 2. Calculated Contact ERH Values and Observed Immersion ERH Values

metal oxide vs AS	contact ERH (%) <sup>a</sup>	immersion ERH (%) <sup>a</sup>	$_{\left(nm\right)^b}^{diameter}$	refs (and values) for previous immersion efflorescence studies
$V_2O_5$	$39 \pm 1$	$37 \pm 2$	90	
CuO	$47 \pm 3$	$38 \pm 3$	65	
ZnO	$48 \pm 3$	$36 \pm 4$	55	
$Fe_2O_3$	$57 \pm 7$	$36 \pm 2$	310	48,49 (35-60% RH)
$TiO_2$	$68 \pm 8$	$37 \pm 3$	310	27,48 (65% RH)

<sup>&</sup>quot;Discussion of error can be found in the Supporting Information.

b Diameters were recovered from the mode values from the SMPS scans seen in Figure S1.

oxide induces contact efflorescence of ammonium sulfate at the highest relative humidity value, signifying that it is the "best" of the observed heterogeneous nuclei, while vanadium (V) oxide leads to the lowest CERH value. It is currently unknown why the heterogeneous nuclei with lower CERH appear to have steeper sigmoid curves, while metal oxides with greater CERH have shallower curves. For this data set, the slopes appear to be steeper at lower RH, and thus higher supersaturation.

However, this may not be generally true for all systems.<sup>8</sup> The shallower slopes lead to larger uncertainty in the calculated CERH at higher relative humidity.

For each metal oxide, experiments were also performed to discern whether or not immersion efflorescence events would occur. A levitated ammonium sulfate droplet was impacted with metal oxide particles at a sufficiently humid RH such that contact efflorescence would not occur, and thus the heterogeneous particles would become immersed inside the aqueous droplet. For each of the five metal oxides observed in this study, the droplet containing approximately three metal oxide nanoparticles did not efflorescence until reaching the homogeneous efflorescence RH of ammonium sulfate within error  $(36 \pm 2\%$ ; see Table 2), implying that the insoluble metal oxides at this level were not able to induce a meaningful immersion efflorescence event. Thus, it is clear that the same metal oxide particles are more effective in causing nucleation in the contact mode than in the immersion mode. This trend has been observed previously; for example, Davis and Tolbert observed that aqueous salt droplets could experience contact efflorescence upon collision with charged polystyrene latex (PSL) particles but would not effloresce if the PSLs and salt solutions were internally mixed.8 Thus, as suggested by that study, efflorescence by these metal oxide nanoparticles may require a hydration-mediated nucleation pathway requiring nonequilibrium conditions that only follow a collision.

Table 2 includes results from previous studies of immersion efflorescence of ammonium sulfate via iron oxide and titanium oxide. Han and Martin report that inclusions of TiO<sub>2</sub> can raise the ERH value of ammonium sulfate up to 65%, while Martin et al. report that inclusions of hematite (Fe2O3) can raise the ERH value of AS up to 60%. These values are both consistent with the ERH values we report here for contact efflorescence but are not comparable with our reported immersion ERH values. It is possible that the difference arises in the quantity of immersed HN in the droplet; Ushijima et al. displayed that the effect of immersion efflorescence on ammonium sulfate depends partially on the total immersed surface area of the mineral dust illite, where the immersion ERH increases with immersed surface area. Han and Martin report particles with a 500 nm metal oxide with 700 nm coating of dry AS. Assuming that the metal oxides and the AS are spherical, the immersed surface area per total volume is equal to 0.785  $\mu$ m<sup>2</sup> in 3.59  $\mu$ m<sup>3</sup>, or 0.219  $\mu$ m<sup>2</sup>/ $\mu$ m<sup>3</sup>. In contrast, each droplet in our study contains approximately three immersed particles with mode diameters as high as 310 nm, as can be seen in Figure S1, with AS droplets with diameters of approximately 15  $\mu$ m. We thus estimate the immersed surface area less than or equal to 0.9  $\mu$ m<sup>3</sup> in a droplet of 1770  $\mu$ m<sup>3</sup>, or 5 × 10<sup>-4</sup>  $\mu$ m<sup>2</sup>/ $\mu$ m<sup>3</sup>. Our immersed quantity is orders of magnitude lower than that of Han and Martin, and so the effects on heterogeneous ERH are not directly comparable. We chose this lower quantity of immersed droplets to directly compare the effects of immersion efflorescence with those of contact efflorescence. It is likely that increasing the immersed surface areas of these metal oxide particles could have a more substantial effect on heterogeneous efflorescence behavior.

While our study did not investigate immersion freezing, an interestingly similar trend has been reported in studies of immersion freezing by ice-nucleating proteins, in which higher concentrations of immersed protein produces a higher fraction of frozen droplets.<sup>50</sup> Similar to ice nucleation, it has been suggested in previous work that a greater match between the

crystal lattice structures of the HN and the salt droplet leads to a higher probability of heterogeneous crystal nucleation, due to an exaggerated mismatch preventing epitaxial growth. However, this does not appear to be true for the insoluble metal oxide particles observed in this study with ammonium sulfate. There is virtually no correlation observed between the crystal lattice match and the contact efflorescence behavior of the metal oxides with ammonium sulfate (see Figure S4). Lattice match with AS was calculated in the same fashion as was done with ice crystals in Section 3.1. This breaks with previous patterns observed between ammonium sulfate and soluble salts as well as with some mineral dust compounds, where a moderate correlation could be seen below a certain mismatch value. 6,9

Previous work done by Davis and Tolbert observes that contact efflorescence may come about due to a transient ion-specific destabilization of the aqueous phase upon collision at the droplet surface. It was seen that ions that more readily approach a hydrophobic, charged surface (e.g., NH<sub>4</sub><sup>+</sup>) will display a lower transient increase in free energy, consistent with lower CERH values. As such, it is considered that this trend in ionic effects may play a role with these colloidal metal oxide nanoparticles as well.

Figure 6 shows the CERH as a function of the cationic metals' oxidation state. There appears to be a linear trend

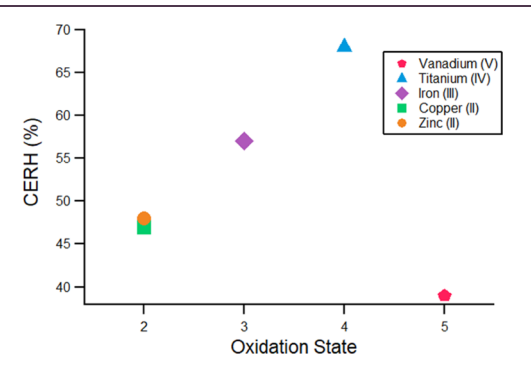


**Figure 6.** CERH of AS upon contact with each metal oxide, as a function of the oxidation state of the metal cation of the contact nucleus.

among four of the five metal oxides. We posit that such a trend may arise due to cationic sites on the metal oxide surface. In particular, coordinatively unsaturated metal cation sites are known to influence adsorption at metal oxide surfaces. 43 In this instance, a higher oxidation state might lead to stronger surface interaction with sulfate ions at cationic sites on the metal oxide surface. However, the CERH value of vanadium (V) oxide was an outlier from this purported trend. It can be theorized that the low CERH of the vanadium oxide, which breaks the trend, is due to the low point of zero charge (PZC) for this metal oxide. Here, PZC is defined as the pH at which the surface potential on a colloidal particle is neutral, comparable to the isoelectric point.<sup>51</sup> At a pH above the PZC, metal oxides will have a negative surface potential; at a pH below the PZC, metal oxides have a positive surface potential. The PZC values for the metal oxides used in this study can be found in Table

The Extended Aerosols Inorganic Model predicts that bulk aqueous ammonium sulfate at 50% RH will have a pH of approximately 4 ( $[H^+]$  = 1.72 × 10<sup>-4</sup> m).<sup>52</sup> Because the PZC of vanadium oxide is reportedly pH 3.2, *i.e.*, below the

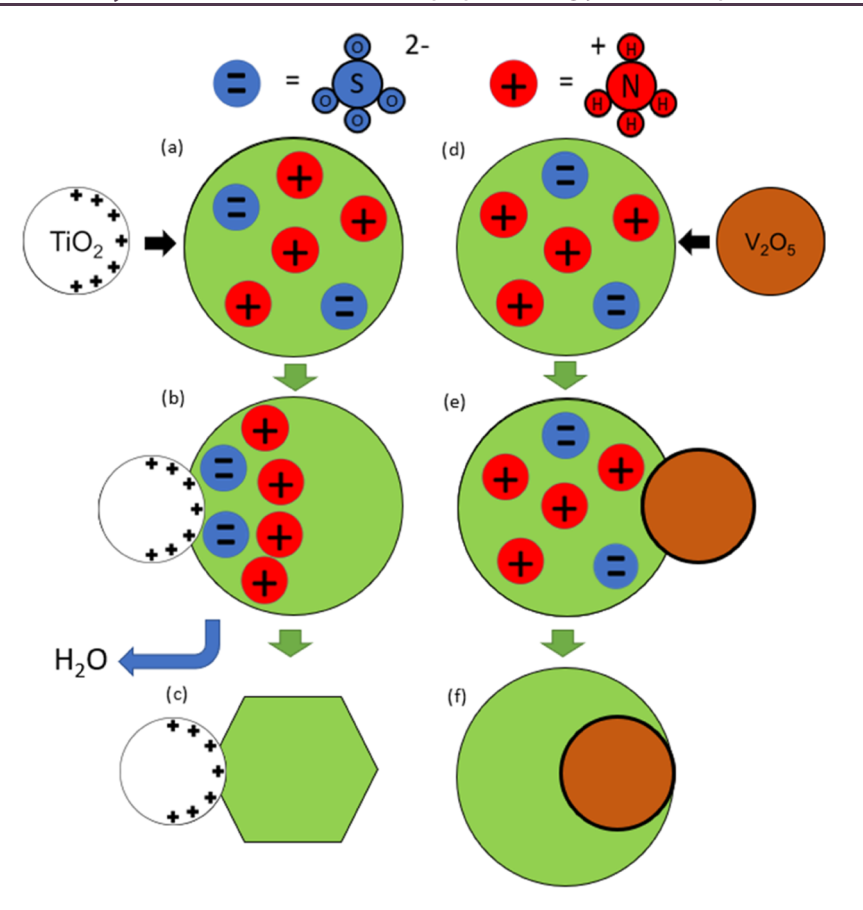


Figure 7. (a–c) Contact between a particle of  $TiO_2$  (white) and a droplet of AS (green). Due to the high PZC and high oxidation state of the metal oxide, transient ionic effects are observed at the surface (b), resulting in an efflorescence event (c). (d–f) Contact between  $V_2O_5$  (brown) and an ammonium sulfate droplet. We posit that the low PZC of  $V_2O_5$  results in few if any transient ionic effects, allowing for continued stability of the aqueous phase (f). Adapted from Davis and Tolbert. For clarity, AS ions are not shown in (c) or (f).

predicted pH of the ammonium sulfate droplet, vanadium oxide may be expected to have a neutral or slightly negative surface potential after colliding with the ammonium sulfate droplet. In contrast, the other metal oxides have PZC values in the pH range of ca. 6–8 in bulk aqueous solution (see Table S2), above the pH of the droplet, and therefore might have a stronger positive surface potential. Although the presence of ammonium and sulfate ions will likely shift the PZC to some extent and the exact surface potential cannot be readily determined from bulk measurements, it may be that the low observed CERH for vanadium oxide is due to the low surface potential, which results in no net attraction of sulfate ions.

Figure 7 shows the hypothesized surface interactions that occur at the surface of an ammonium sulfate droplet upon collision with the HN. An HN with a PZC above the droplet's pH, such as TiO<sub>2</sub>, would have a positive surface potential and would interact strongly with the sulfate in solution, leading to a phase-change event via destabilization of the aqueous phase. However, the vanadium oxide, with a PZC slightly below the droplet's pH, would have a weakly negative surface potential and would interact weakly with the ammonium in solution, and therefore be less successful in disrupting the aqueous phase. Further, in the instance where ammonium is attracted to the surface by a net surface potential, the primary ion-surface interaction will not involve the metal cations, which could further explain why vanadium is an outlier, i.e., metal sites and coordinatively unsaturated metal sites are not influencing efflorescence in the specific case of  $V_2O_5$ .

In previous work, Davis and Tolbert showed that a contact nucleus with a negatively charged surface was less effective at inducing contact efflorescence when ammonium was the cation in solution. Because ammonium is more stable approaching a negative particle surface, the aqueous phase experiences less disturbance and is therefore less likely to induce a phase-change event. Our observation that vanadium oxide is less effective as a contact nucleus is consistent with this previous conclusion since vanadium likely has a neutral to slightly negative surface.

While the contact efflorescence behavior of the metal oxides did not follow previous trends regarding crystal lattice match, a possible trend has been identified regarding ion-surface interactions at cationic metal sites, further supporting the theory put forward by Davis and Tolbert that contact efflorescence is dependent on transient ionic effects.<sup>8</sup>

## 4. CONCLUSIONS

Contrary to some previous studies, the match of crystal lattice structures between these five metal oxide heterogeneous nuclei (HN) and ice crystals did not seem to be an acceptable predictor of the effectiveness of depositional ice nucleation on the metal oxides. Likewise, the lattice match between HN and salt crystal was not a reasonable predictor of the effectiveness of contact efflorescence. The predictors of nucleation are highly complex and deserve attention in future experimental studies and atmospheric models. A trend is observed, however, relating both the ice nucleation efficiency and the contact

efflorescence efficiency with the oxidation state of the transition-metal oxide particle.

Regarding ice nucleation, while the surface charge of the metal oxide agglomerates was not directly measured in this study, the noted correlation between nucleation efficiency and cation oxidation state perhaps deserves future consideration in studies and predictions of ice formation in atmospheric mixedphase clouds.

Considering past studies of contact efflorescence, it is likely that contact efflorescence of AS induced by metal oxides is a transient ion-surface effect.<sup>8,9</sup> Consistent with this, all five heterogeneous nuclei were able to cause contact efflorescence of ammonium sulfate in some respect but were unable to promote immersion efflorescence at an RH significantly different than that of homogeneous efflorescence. The trends discovered here regarding oxidation state and ion effects may help to elucidate how these insoluble metal oxides cause collisional efflorescence and may guide the predicted behavior of salt aerosol droplets in atmospheric conditions.

#### ASSOCIATED CONTENT

# Supporting Information

The Supporting Information is available free of charge at https://pubs.acs.org/doi/10.1021/acsearthspacechem.2c00370.

> Discussion of error propagation; size distribution profiles for the five metal oxides (Figure S1); Raman spectra and microscope imaging for the five metal oxides (Figure S2); discussion of crystal lattice mismatch calculation; lattice constants utilized to calculate lattice mismatch values (Table S1); ice saturation as a function of crystal lattice match with ice (Figure S3); CERH values of ammonium sulfate for each metal oxide plotted against that oxide's respective lattice mismatch with ammonium sulfate (Figure S4); and PZC values for each metal oxide (Table S2) (PDF)

# AUTHOR INFORMATION

## **Corresponding Author**

Margaret A. Tolbert - Cooperative Institute for Research in Environmental Sciences, University of Colorado, Boulder, Colorado 80309, United States; Department of Chemistry, University of Colorado, Boulder, Boulder, Colorado 80309, *United States;* orcid.org/0000-0001-5730-6412; Phone: (303) 492-3179; Email: margaret.tolbert@ colorado.edu

# **Authors**

**Zachary R. Schiffman** – Cooperative Institute for Research in Environmental Sciences, University of Colorado, Boulder, Colorado 80309, United States; Department of Chemistry, University of Colorado, Boulder, Boulder, Colorado 80309, United States; orcid.org/0000-0002-7240-4739

Marium S. Fernanders - Cooperative Institute for Research in Environmental Sciences, University of Colorado, Boulder, Colorado 80309, United States; Department of Chemistry, University of Colorado, Boulder, Boulder, Colorado 80309, *United States*; orcid.org/0000-0002-1327-4321

Ryan D. Davis – Sandia National Laboratories, Albuquerque, New Mexico 87123, United States; o orcid.org/0000-0002-4434-1320

Complete contact information is available at:

https://pubs.acs.org/10.1021/acsearthspacechem.2c00370

#### **Author Contributions**

The manuscript was written through contributions of all authors. All authors have given approval to the final version of the manuscript.

#### Notes

The authors declare no competing financial interest.

# ACKNOWLEDGMENTS

Z.R.S. was supported in part by the CIRES Graduate Student Research Award and the NOAA Cooperative Agreement with CIRES, NA17OAR4320101. This work was also supported in part by NSF grant AGS 1925191. Sandia National Laboratories is a multimission laboratory managed and operated by National Technology & Engineering Solutions of Sandia, LLC, a wholly owned subsidiary of Honeywell International Inc., for the U.S. Department of Energy's National Nuclear Security Administration under contract DE-NA0003525. This paper describes objective technical results and analysis. Any subjective views or opinions that might be expressed in the paper do not necessarily represent the views of the U.S. Department of Energy or the United States Government.

# ABBREVIATIONS

 $\delta$ , lattice mismatch parameter  $\mu$ m, micrometer Cu, copper Fe. Iron Ti, titanium V, vanadium Zn, zinc AS, ammonium sulfate, or  $(NH_4)_2SO_4$ CCD, charge-coupled device CERH, relative humidity of contact efflorescence CPC, condensation particle counter DMA, differential mobility analyzer ERH, relative humidity of efflorescence HN, heterogeneous nucleus (or nuclei) PSL, polystyrene latex

PZC, point of zero charge RH, relative humidity

S<sub>ice</sub>, onset ice saturation ratio SMPS, scanning mobility particle sizer

# REFERENCES

- (1) Tang, M.; Cziczo, D. J.; Grassian, V. H. Interactions of Water with Mineral Dust Aerosol: Water Adsorption, Hygroscopicity, Cloud Condensation, and Ice Nucleation. Chem. Rev. 2016, 116, 4205-
- (2) Ginoux, P.; Prospero, J. M.; Gill, T. E.; Hsu, N. C.; Zhao, M. Global-scale attribution of anthropogenic and natural dust sources and their emission rates based on MODIS Deep Blue aerosol products. Rev. Geophys. 2012, 50, No. RG3005.
- (3) Lambert, A.; Hallar, A. G.; Garcia, M.; Strong, C.; Andrews, E.; Hand, J. L. Dust impacts of rapid agricultural expansion on the Great Plains. Geophys. Res. Lett. 2002, 47, No. e2020GL090347.
- (4) Charlson, R. J.; Schwartz, S. E.; Hales, J. M.; Cess, R. D.; Coakley, J. A.; Hansen, J. E.; Hofmann, D. J. Climate forcing by anthropogenic aerosols. Science 1992, 255, 423-430.
- (5) Cziczo, D. J.; Froyd, K. D.; Hoose, C.; Jensen, E. J.; Diao, M.; Zondlo, M. A.; Smith, J. B.; Twohy, C. H.; Murphy, D. M. Clarifying the dominant sources and mechanisms of cirrus cloud formation. Science 2013, 340, 1320-1324.

- (6) Davis, R. D.; Lance, S.; Gordon, J. A.; Ushijima, S. B.; Tolbert, M. A. Contact efflorescence as a pathway for crystallization of atmospherically relevant particles. *Proc. Natl. Acad. Sci. U.S.A.* **2015**, *112*, 15815–15820.
- (7) Davis, R. D.; Lance, S.; Gordon, J. A.; Tolbert, M. A. Long Working-Distance Optical Trap for in Situ Analysis of Contact-Induced Phase Transformations. *Anal. Chem.* **2015**, *87*, 6186–6194.
- (8) Davis, R. D.; Tolbert, M. A. Crystal nucleation initiated by transient ion-surface interactions at aerosol interfaces. *Sci. Adv.* **2017**, 3, No. e1700425.
- (9) Ushijima, S. B.; Davis, R. D.; Tolbert, M. A. Immersion and Contact Efflorescence Induced by Mineral Dust Particles. *J. Phys. Chem. A* **2018**, *122*, 1303–1311.
- (10) Ushijima, S. B.; Gough, R. V.; Tolbert, M. A. Probing Heterogeneous Efflorescence of Mars-Relevant Salts with an Optical Levitator. *ACS Earth Space Chem.* **2020**, *4*, 1947–1956.
- (11) Ushijima, S. B.; Huynh, E.; Davis, R. D.; Tolbert, M. A. Seeded Crystal Growth of Internally Mixed Organic-Inorganic Aerosols: Impact of Organic Phase State. *J. Phys. Chem. A* **2021**, *125*, 8668–8679.
- (12) Archuleta, C. M.; DeMott, P. J.; Kreidenweis, S. M. Ice nucleation by surrogates for atmospheric mineral dust and mineral dust/sulfate particles at cirrus temperatures. *Atmos. Chem. Phys.* **2005**, *5*, 2617–2634.
- (13) Ladino Moreno, L. A.; Stetzer, O.; Lohmann, U. Contact freezing: a review of experimental studies. *Atmos. Chem. Phys.* **2013**, 13, 9745–9769.
- (14) Hoose, C.; Kristjánsson, J. E.; Chen, J.-P.; Hazra, A. A Classical-Theory-Based Parameterization of Heterogeneous Ice Nucleation by Mineral Dust, Soot, and Biological Particles in a Global Climate Model. *J. Atmos. Sci.* **2010**, *67*, 2483–2503.
- (15) Broadley, S. L.; Murray, B. J.; Herbert, R. J.; Atkinson, J. D.; Dobbie, S.; Malkin, T. L.; Condliffe, E.; Neve, L. Immersion mode heterogeneous ice nucleation by an illite rich powder representative of atmospheric mineral dust. *Atmos. Chem. Phys.* **2012**, *12*, 287–307.
- (16) Diehl, K.; Debertshäuser, M.; Eppers, O.; Schmithüsen, H.; Mitra, S. K.; Borrmann, S. Particle surface area dependence of mineral dust in immersion freezing mode: investigations with freely suspended drops in an acoustic levitator and a vertical wind tunnel. *Atmos. Chem. Phys.* **2014**, *14*, 12343–12355.
- (17) Wheeler, M. J.; Mason, R. H.; Steunenberg, K.; Wagstaff, M.; Chou, C.; Bertram, A. K. Immersion Freezing of Supermicron Mineral Dust Particles: Freezing Results, Testing Different Schemes for Describing Ice Nucleation, and Ice Nucleation Active Site Densities. J. Phys. Chem. A 2015, 119, 4358–4372.
- (18) Eastwood, M. L.; Cremel, S.; Gehrke, C.; Girard, E.; Bertram, A. K. Ice nucleation on mineral dust particles: Onset conditions, nucleation rates and contact angles. *J. Geophys. Res.* **2008**, *113*, D22203.
- (19) Yakobi-Hancock, J. D.; Ladino, L. A.; Abbatt, J. P. D. Feldspar minerals as efficient deposition ice nuclei. *Atmos. Chem. Phys.* **2013**, 13, 11175–11185.
- (20) Atkinson, J. D.; Murray, B. J.; Woodhouse, M. T.; Whale, T. F.; Baustian, K. J.; Carslaw, K. S.; Dobbie, S.; O'Sullivan, D.; Malkin, T. L. The importance of feldspar for ice nucleation by mineral dust in mixed-phase clouds. *Nature* **2013**, *498*, 355–358.
- (21) Harrison, A. D.; Whale, T. F.; Carpenter, M. A.; Holden, M. A.; Neve, L.; O'Sullivan, D.; Temprado, J. V.; Murray, B. J. Not all feldspars are equal: a survey of ice nucleating properties across the feldspar group of minerals. *Atmos. Chem. Phys.* **2016**, *16*, 10927–10940.
- (22) Paramonov, M.; David, R. O.; Kretzschmar, R.; Kanji, Z. A. A laboratory investigation of the ice nucleation efficiency of three types of mineral and soil dust. *Atmos. Chem. Phys.* **2018**, *18*, 16515–16536.
- (23) Marcolli, C. Deposition nucleation viewed as homogeneous or immersion freezing in pores and cavities. *Atmos. Chem. Phys.* **2014**, *14*, 2071–2104.
- (24) David, R. O.; Marcolli, C.; Fahrni, J.; Qiu, Y.; Sirkin, Y. A. P.; Molinero, V.; Mahrt, F.; Brühwiler, D.; Lohmann, U.; Kanji, Z. A.

- Pore condensation and freezing is responsible for ice formation below water saturation for porous particles. *Proc. Natl. Acad. Sci. U.S.A.* **2019**, *116*, 8184–8189.
- (25) Holden, M. A.; Campbell, J. M.; Meldrum, F. C.; Murray, B. J.; Christenson, H. K. Active sites for ice nucleation differ depending on nucleation mode. *Proc. Natl. Acad. Sci. U.S.A.* **2021**, *118*, No. e2022859118.
- (26) Kiselev, A.; Bachmann, F.; Pedevilla, P.; Cox, S. J.; Michaelides, A.; Gerthsen, D.; Leisner, T. Active sites in heterogeneous ice nucleation—the example of K-rich feldspars. *Science* **2017**, *355*, 367–371.
- (27) Han, J.-H.; Martin, S. T. Heterogeneous nucleation of the efflorescence of (NH4)2SO4 particles internally mixed with Al2O3, TiO2, and ZrO2. *J. Geophys. Res.* **1999**, *104*, 3543–3553.
- (28) Lafuente, B.; Downs, R. T.; Yang, H.; Stone, N. The Power of Databases: The RRUFF Project. In *Highlights in Mineralogical Crystallography*; Armbuster, T.; Danisi, R. M., Eds.; W. De Gruyter: Germany, 2015.
- (29) Shvets, P.; Dikaya, O.; Maksimova, K.; Goikhman, A. A review of Raman spectroscopy of vanadium oxides. *J. Raman Spectrosc.* **2019**, 50, 1226–1244.
- (30) Hanesch, M. Raman spectroscopy of iron oxides and (oxy)hydroxides at low laser power and possible applications in environmental magnetic studies. *Geophys. J. Int.* **2009**, *177*, 941–948.
- (31) Fernanders, M. S.; Gough, R. V.; Chevrier, V. F.; Schiffman, Z. R.; Ushijima, S. B.; Martinez, G. M.; Rivera-Valentín, E. G.; Archer, P. D., Jr.; Clark, J. V.; Sutter, B.; Tolbert, M. A. Water uptake by chlorate salts under Mars-relevant conditions. *Icarus* **2022**, *371*, No. 114715.
- (32) Baustian, K. J.; Wise, M. E.; Tolbert, M. A. Depositional ice nucleation on solid ammonium sulfate and glutaric acid particles. *Atmos. Chem. Phys.* **2010**, *10*, 2307–2317.
- (33) Koop, T.; Luo, B.; Tsias, A.; Peter, T. Water activity as the determinant for homogeneous ice nucleation in aqueous solutions. *Nature* **2000**, *406*, 611–614.
- (34) Knopf, D. A.; Koop, T. Heterogeneous nucleation of ice on surrogates of mineral dust. *J. Geophys. Res.* **2006**, *111*, D12201.
- (35) Salam, A.; Lohmann, U.; Crenna, B.; Lesins, G.; Klages, P.; Rogers, D.; Irani, R.; MacGillivray, A.; Coffin, M. Ice nucleation studies of mineral dust particles with a new continuous flow diffusion chamber. *Aerosol Sci. Technol.* **2006**, *40*, 134–143.
- (36) Schill, G. P.; De Haan, D. O.; Tolbert, M. A. Heterogeneous Ice Nucleation on Simulated Secondary Organic Aerosol. *Environ. Sci. Technol.* **2014**, *48*, 1675–1682.
- (37) Kuo, T.-H.; Murakami, M.; Tajiri, T.; Orikasa, N. Cloud Condensation Nuclei and Immersion Freezing Abilities of Al2O3 and Fe2O3 Particles Measured with the Meteorological Research Institute's Cloud Simulation Chamber. *J. Meteorol. Soc. Jpn. Ser. II* **2019**, *97*, 597–614.
- (38) Saunders, R. W.; Mohler, O.; Schnaiter, M.; Benz, S.; Wagner, R.; Saathoff, H.; Connolly, P. J.; Burgess, R.; Murray, B. J.; Gallagher, M.; Wills, R.; Plane, J. M. C. An aerosol chamber investigation of the heterogeneous ice nucleating potential of refractory nanoparticles. *Atmos. Chem. Phys.* **2010**, *10*, 1227–1247.
- (39) Pruppacher, R.; Klett, J. D. Microphysics of Clouds and Precipitation; Kluwer Academic Publishers, 1997.
- (40) Fitzner, M.; Pedevilla, P.; Michaelides, A. Predicting heterogeneous ice nucleation with a data-driven approach. *Nat. Commun.* **2020**, *11*, No. 4777.
- (41) Glatz, B.; Sarupria, S. The surface charge distribution affects the ice nucleating efficiency of silver iodide. *J. Chem. Phys.* **2016**, *145*, No. 211924.
- (42) Zielke, S. A.; Bertram, A. K.; Patey, G. N. A Molecular Mechanism of Ice Nucleation on Model AgI Surfaces. *J. Phys. Chem. B.* **2015**, *119*, 9049–9055.
- (43) Mu, R.; Zhao, Z.-J.; Dohnalek, Z.; Gong, J. Structural motifs of water on metal oxide surfaces. Chem. Soc. Rev. 2017, 46, 1785–1806.
- (44) Kumar, A.; Marcolli, C.; Luo, B.; Peter, T. Ice nucleation activity of silicates and aluminosilicates in pure water and aqueous

- solutions Part 1: The K-feldspar microcline. *Atmos. Chem. Phys.* **2018**, *18*, 7057–7079.
- (45) Kumar, A.; Marcolli, C.; Peter, T. Ice nucleation activity of silicates and aluminosilicates in pure water and aqueous solutions Part 2: Quartz and amorphous silica. *Atmos. Chem. Phys.* **2019**, *19*, 6035–6058.
- (46) Kumar, A.; Marcolli, C.; Peter, T. Ice nucleation activity of silicates and aluminosilicates in pure water and aqueous solutions Part 3: Aluminosilicates. *Atmos. Chem. Phys.* **2019**, *19*, 6059–6084.
- (47) Worthy, S. E.; Kumar, A.; Xi, Y.; Yun, J.; Chen, J.; Xu, C.; Irish, V. E.; Amato, P.; Bertram, A. K. The effect of (NH4)2SO4 on the freezing properties of non-mineral dust ice-nucleating substances of atmospheric relevance. *Atmos. Chem. Phys.* **2021**, 21, 14631–14648.
- (48) Martin, S. T.; Schlenker, J.; Chelf, J. H.; Duckworth, O. W. Structure—Activity Relationships of Mineral Dusts as Heterogeneous Nuclei for Ammonium Sulfate Crystallization from Supersaturated Aqueous Solutions. *Environ. Sci. Technol.* **2001**, *35*, 1624–1629.
- (49) Martin, S. T.; Han, J.-H.; Hung, H.-M. The size effect of hematite and corundum inclusions on the efflorescence relative humidities of aqueous ammonium sulfate particles. *Geophys. Res. Lett.* **2001**, 28, 2601–2604.
- (50) Cascajo-Castresana, M.; David, R. O.; Iriarte-Alonso, M. A.; Bittner, A. M.; Marcolli, C. Protein aggregates nucleate ice: the example of apoferritin. *Atmos. Chem. Phys.* **2020**, *20*, 3291–3315.
- (51) Sposito, G. On Points of Zero Charge. Environ. Sci. Technol. 1998, 32, 2815-2819.
- (52) Wexler, A. S.; Clegg, S. L. Atmospheric aerosol models for systems including the ions H+, NH4+, Na+, SO42-, NO3-, Cl-, Br-, and H2O. *J. Geophys. Res.* **2002**, *107* (D14), 4207.